Available online at www.sciencedirect.com

ScienceDirect

Proceedings of the Combustion Institute 37 (2019) 667–675

Proceedings of the Combustion Institute

www.elsevier.com/locate/proci

The sensitizing effects of NO_2 and NO on methane low temperature oxidation in a jet stirred reactor

Y. Song [a], L. Marrodán [b], N. Vin [a], O. Herbinet [a,*], E. Assaf [c], C. Fittschen [c], A. Stagni [d], T. Faravelli [d], M.U. Alzueta [b], F. Battin-Leclerc [a]

[a] *Laboratoire Réactions et Génie des Procédés, CNRS-Université de Lorraine, 1 rue Grandville, 54000 Nancy, France*

[b] *Aragón Institute of Engineering Research (I3A), Department of Chemical and Environmental Engineering, University of Zaragoza, Mariano Esquillor s/n, 50018 Zaragoza, Spain*

[c] *Université Lille, CNRS, UMR 8522- PC2A-PhysicoChimie des Processus de Combustion et de l'Atmosphère, F59000 Lille, France*

[d] *Department of Chemistry, Materials and Chemical Engineering "G. Natta", Politecnico di Milano, Piazza Leonardo da Vinci 32, 20133 Milano, Italy*

Received 29 November 2017; accepted 18 June 2018
Available online 3 July 2018

Abstract

The oxidation of neat methane (CH_4) and CH_4 doped with NO_2 or NO in argon has been investigated in a jet-stirred reactor at 107 kPa, temperatures between 650 and 1200 K, with a fixed residence time of 1.5 s, and for different equivalence ratios (Φ), ranging from fuel-lean to fuel-rich conditions. Four different diagnostics have been used: gas chromatography (GC), chemiluminescence NO_x analyzer, continuous wave cavity ring-down spectroscopy (cw-CRDS) and Fourier transform infrared spectroscopy (FTIR). In the case of the oxidation of neat methane, the onset temperature for CH_4 oxidation was above 1025 K, while it is shifted to 825 K with the addition of NO_2 or NO, independently of equivalence ratio, indicating that the addition of NO_2 or NO highly promotes CH_4 oxidation. The consumption rate of CH_4 exhibits a similar trend with the presence of both NO_2 and NO. The amount of produced HCN has been quantified and a search for HONO and CH_3NO_2 species has been attempted. A detailed kinetic mechanism, derived from POLIMI kinetic framework, has been used to interpret the experimental data with a good agreement between experimental data and model predictions. Reaction rate and sensitivity analysis have been conducted to illustrate the kinetic regimes. The fact that the addition of NO or NO_2 seems to have similar effects on promoting CH_4 oxidation can be explained by the fact that both species are involved in a reaction cycle interchanging them and whose result is $2CH_3 + O_2 = 2CH_2O + 2H$. Additionally, the direct participation of NO_2 in the $NO_2 + CH_2O = HONO + HCO$ reaction has a notable accelerating effect on methane oxidation.

Keywords: Jet-stirred reactor; NO_x methane combustion; Low-temperature oxidation

https://doi.org/10.1016/j.proci.2018.06.115

1. Introduction

The limited fossil fuel resource and its harmful effects on the climate have increased the interest for environmentally friendly fuels. Biomass seems to be a promising fuel source due to its sustainability, secure supply and low threat to the environment. Produced from the biomass anaerobic digestion, the so-called "biogas", consists mainly of methane (CH_4) and carbon dioxide (CO_2) with trace amounts of nitrogen and sulfur compounds. Biogas plays an important role as potential renewable gas-phase fuel. The main nitrogen compound present in biogas is ammonia, which could easily convert to NO in the presence of oxygen even at low temperatures. The mutual effects of CH_4/NO_x or CH_4/NH_3 have attracted considerable attention in the past decade.

A large number of experimental reports concerning the hydrocarbon-NO_x interactions in ideal reactors are available [1–12]. Most studies related to reburning technology were performed in tubular flow reactors (FR) for CH_4 high-temperature oxidation. Over a relatively low-temperature range (800–1150 K), Dagaut and Nicolle [6] demonstrated the effects of NO on methane oxidation at pressures of 1–10 atm in a jet stirred reactor. A simplified reaction path was proposed, in which the reaction $NO + HO_2 = OH + NO_2$ followed by $OH + CH_4 = CH_3 + H_2O$ were highlighted. In addition, the investigation of mutual effects of NO_2 on CH_4 oxidation is also of significant value. Bendtsen et al. [4] and Chan et al. [9] examined the impact of NO and NO_2 as promoters to CH_4 oxidation under fuel-lean conditions in a FR. The different key reactions at the onset for NO ($CH_3O_2 + NO = CH_3O + NO_2$) or NO_2 ($NO_2 + CH_4 = CH_3 + HONO$) sensitization were identified. However, some minor reaction paths such as $NO_2 + CH_2O = HONO + HCO$, which could play a role in mutual effects on CH_4 oxidation, have been ignored so far. Moreover, to the authors' knowledge, the sensitizing effects of NO_2 on methane low-temperature oxidation in a jet-stirred reactor have not been investigated yet.

Despite the abundant kinetic studies for the CH_4–NO_x interactions, the knowledge of some notable intermediate nitrogen species (such as HONO) is not comprehensively understood. Chai and Goldsmith [13] calculated the rate coefficients for $H_2 + NO_2$ and $CH_4 + NO_2$ with the formation of HONO. The fate of these species is of importance to the hydrocarbon-NO_x interactions during the biogas oxidation. However, until now, HONO has never been detected during fuel oxidation.

Therefore, the aim of this work is to investigate the hydrocarbon-NO_x (NO and NO_2) interactions in biogas oxidation at atmospheric pressure and temperatures ranging from 650 to 1200 K. A search for intermediate species HONO, CH_3NO_2 and HCN has been made with the aid of continuous wave Cavity Ring-Down Spectroscopy (cw-CRDS) and Fourier Transform Infrared (FTIR), respectively. A detailed kinetic mechanism, recently updated according to the latest available *ab initio* calculations, is used to interpret the experimental data.

2. Experimental setup

The experimental setup was a laboratory-scale spherical fused silica JSR (volume of 85 cm^3; detailed description provided elsewhere [14]). A more detailed description of the experimental setup is available in Supplementary material (SM1). The reactant gases were premixed in a preheating zone before entering the reactor center through four nozzles which create high turbulence resulting in homogeneity in composition and temperature of the gas phase. The residence time inside the preheater was only 1% with respect to the one in the reactor which was fixed at 1.5 s (±0.1 s) within all the experiments performed. Both the reactor and the preheater were heated using Thermocoax resistances. The reactor temperature was measured by a type-K thermocouple (±5 K) located at the center of the reactor. The pressure in the reactor was controlled by a needle valve (±0.2 kPa) positioned downstream of the reactor and kept at 107 kPa. Argon, oxygen, NO, NO_2 and methane were provided by Messer (purities of 99.99%, respectively). The flow rates of the reactants were controlled by mass flow controllers (±0.05%). The gases leaving the reactor were analyzed on-line using two gas chromatographs (GCs), a NO_x analyzer (Thermo Scientific Model 42i), a FTIR (Thermo Scientific Antaris) spectrometer and a cw-CRDS spectroscopy cell.

- The first GC equipped with a thermal conductivity detector was used to quantify O_2. The second GC equipped with flame-ionization detector preceded by a methanizer and a PlotQ capillary column was used to quantify CH_4, CO, CO_2, C_2H_4, C_2H_6 and C_2H_2.
- The chemiluminescence NO_x analyzer was adopted to measure NO and NO_2. The quantitative range is 0–5000 ppm for NO and 0–500 ppm for NO_2 with 0.1 ppm sensitivity, respectively. Two pumps are used for outlet and bypass channels, respectively.
- The FTIR spectrometer was used to detect the CH_3NO_2 (if any) and HCN (calibrated using a HCN diluted (1000 ppm in N_2) cylinder) species.

* Corresponding author.
E-mail address: olivier.herbinet@univ-lorraine.fr (O. Herbinet).

- cw-CRDS infrared spectroscopy was used to detect H_2O, CH_2O and HONO (if any) species, the description of this instrument is also provided in [15].

The uncertainty for the different diagnostic instruments is estimated to be ±5% except for the FTIR and CRDS measurements which is ±10–15%. All the experimental data presented hereafter are detailed in a spreadsheet in SM2.

3. Kinetic model

The kinetic mechanism used for chemistry description and analysis of experimental results was obtained by relying on the POLIMI kinetic framework, describing the pyrolysis and oxidation of hydrocarbon fuels [16]. Its core C_0–C_3 mechanism was recently revised by coupling the H_2/O_2 and C_1/C_2 subsets from Metcalfe et al. [17], C_3 from Burke et al. [18], and heavier fuels from Ranzi et al. [19]. For the low temperature conditions of interest in this work, particular attention was devoted to updating the (equilibrated) reaction rates of peroxy radical formation from methyl radical [20], as well as the related thermodynamic properties. They were adopted, when available, from the database of Burcat and Ruscic [21].

Following the modularity principle behind the POLIMI mechanism, a NO_x sub-mechanism was integrated into the main framework: a complete characterization of its basic structure is provided in [22, 23]. It describes the major paths leading to NO_x formation. Apart from the three well-studied reactions responsible of thermal NO_x mechanism [24], the mechanism underwent a major update for the prompt path, especially in relation to the NCN-route: the kinetic laws of the reactions involving NCN were updated after the *ab initio* calculations by Harding et al. [25] and Faßheber et al. [26]. Moreover, the chemistry of HNC and HNCN was also updated according to the modifications proposed by Lamoureux et al. [27]. On the other side, the high-temperature reburning mechanism of methane implements the rates proposed by Dean and Bozzelli [28] for the reactions of methyl with NO. The methoxy activation by NO ($CH_3O_2 + NO = CH_3O + NO_2$) was obtained from Atkinson et al. [29], and validated in the 200–430 K temperature range, while its direct formation via NO_2 ($CH_3 + NO_2 = CH_3O + NO$) was updated following Glarborg and Bendtsen [30], which is temperature independent over the range 295–1400 K. Rate coefficients of HONO and HNO_2 formation from methane and NO_2 were implemented following Chai and Goldsmith [13]. The complete mechanism (153 species and 2361 reactions) is provided as supplemental material of this paper in CHEMKIN format, along with thermodynamic and transport properties (SM3). The present mechanism is able to reproduce experimental data from literature [6, 7, 9] as shown in SM1.

Table 1
Experimental conditions (Inlet composition volume basis; balanced Ar).

Exp.	X_{CH4}	X_{NO} ppm	X_{NO2} ppm	X_{O2}	Φ
1	0.01	–	–	0.04	0.5
2	0.01	–	–	0.02	1
3	0.01	–	–	0.01	2
4	0.01	500	–	0.04	0.5
5	0.01	500	–	0.02	1
6	0.01	500	–	0.01	2
7	0.01	100	–	0.02	1
8	0.01	–	400	0.04	0.5
9	0.01	–	400	0.02	1
10	0.01	–	400	0.01	2
11	0.01	–	100	0.02	1
12	0.01	1000	–	0.02	1

4. Results

Experiments for the oxidation of CH_4 doped with NO and NO_2 with argon as bath gas were performed under fuel-lean (Φ = 0.5) to fuel-rich (Φ = 2) conditions over the 650–1200 K temperature range. Equivalence ratios were calculated neglecting the amounts of added NO_x compounds which were around 4–10% that of CH_4. The experimental conditions investigated in this study are presented in Table 1. Numerical calculations were conducted with CHEMKIN-PRO software package [31]. Transient solver was applied in the simulation tasks with sufficient time allowed to reach the steady state solution.

4.1. Profiles of carbon compound species and water

Figure 1 shows the evolution of major products with temperature for the oxidation of CH_4 (left), methane doped with NO_2 (middle) and NO (right) for the three studied equivalence ratios (Φ = 0.5, 1 and 2). With respect to the pure CH_4 oxidation, the initial oxidation temperatures are 1025 K, 1075 K and 1175 K for Φ = 0.5, 1 and 2, respectively. Dynamic behaviors (oscillations) occur under oxidizing and stoichiometric conditions when the temperature is above 1050 K and 1100 K, respectively. This is, too, an interesting topic of research in such systems, but beyond the goals of this specific study.

In the presence of NO_2 (400 ppm) under fuel-lean conditions, the reaction is initiated at 825 K. The rise of consumption of CH_4 is extremely fast with the increase of temperature. At 950 K, 98% of the inlet methane concentration was oxidized. Under stoichiometric conditions, the onset temperature for CH_4 oxidation is around 825 K as well. However, CH_4 consumption is slower than that under fuel-lean conditions: there is still 24% CH_4 left

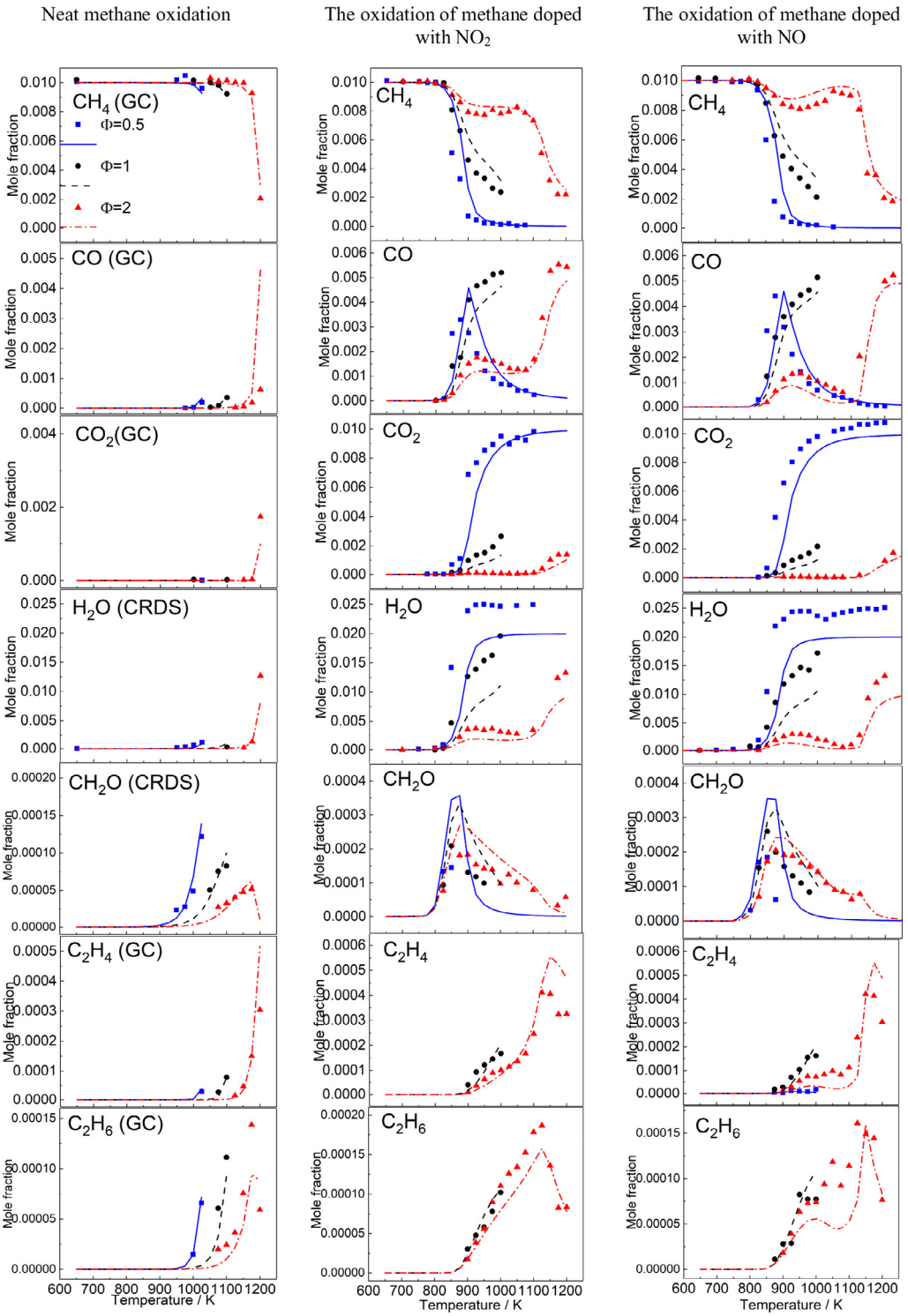

Fig. 1. Species profile comparison between experimental data and model predictions. The left column is for the oxidation of neat methane; the middle column is for the oxidation of methane doped with NO_2 (400 ppm); the right column is for the oxidation of methane doped with NO (500 ppm). Here and in further figures in this paper, symbols represent experiments and lines denote simulations. Experiments and simulations are not presented for conditions where oscillations were observed.

in the reactor outlet at 1000 K. Similarly as under the above two conditions, the consumption of methane also starts at 825 K under fuel-rich conditions, whereas the consumption of methane is even slower compared to that under stoichiometric conditions. Differing from what is observed under stoichiometric and oxidizing conditions, the mole fraction of methane reaches a minimum at 950 K under reducing conditions, and the mole fraction of methane increases at higher temperatures until 1050 K. After that, methane is consumed again. Compared to the oxidation of neat methane (left column), the enhancing effect for the addition of NO_2 into the oxidizing environment system is quite obvious especially for reducing conditions.

In the presence of NO (500 ppm), the evolution of methane profiles is quite similar to what is obtained in the presence of NO_2. This indicates that the promoting effects of NO and NO_2 on methane oxidation is almost the same although the amount of the addition of NO and NO_2 is a little different.

Note that oscillations even occur under stoichiometric ($T > 1100$ K, with NO_2 addition) in the presence of NO and NO_2. The present model could reproduce the above mentioned dynamic behavior as shown in SM1.

The peak mole fraction of CH_2O profile occurs at a temperature of 850 K, which is independent of equivalence ratios in the presence of both NO and NO_2. Likewise, the mole fraction of CO reaches its utmost value at 850 K under fuel-lean conditions, which indicates that the methane oxidation is very fast at this specific temperature. Under fuel-rich conditions, the temperature for the peak CO mole fraction shifts to 900 K. C_2 species (C_2H_4, C_2H_6) mainly appear under stoichiometric and reducing conditions at higher temperature ($T > 900$ K). Under oxidizing conditions, the mole fraction of C_2 species are below the detection limit and this behavior is well captured by the model as is shown in SM1. The global carbon balance has been checked and the deviation is below 5% (SM2).

The agreement between the experimental data and simulated results is generally good within all the investigated conditions except for that the model underestimates the experimental profile of H_2O under stoichiometric and fuel-lean conditions, which was also observed by Bugler et al. [32]. It might be ascribed to the uncertainty in cw-CRDS measurements derived from its significant concentrations. Also, the performance of different literature models against present experimental data is displayed in SM1. It is found that the current POLIMI model is better capturing the experimental data than the other models.

In order to evaluate the effect of the amount of added NO_2 and NO on the methane oxidation, three more sets of experiments with addition of 100 ppm NO_2 or NO and addition of 1000 ppm NO (sets 7,11 and 12 in Table 1), respectively, were conducted. Figure 2 shows both the experimental and model results. It was found that the onset temperature for methane oxidation is independent of the added amount of NO_2 and NO. Moreover, with the lower added amount of NO_2 or NO, the methane conversion is slower. When 1000 ppm of NO is present, methane conversion shows a trend similar to that with 500 ppm NO addition. Furthermore, the consumption rate for methane also exhibits the similar trend in the presence of both NO_2 (100 ppm) and NO (100 ppm) which differs from what was previously observed by Chan et al. [9] in a FR.

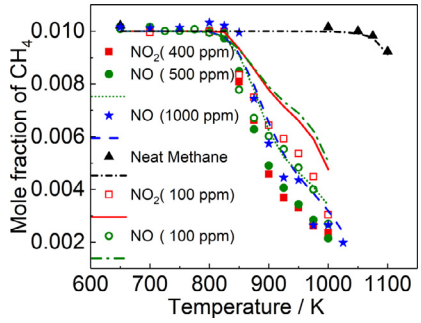

Fig. 2. Mole fractions of methane with various additions of NO_2 (400 and 100 ppm) and NO (1000, 500 and 100 ppm) under stoichiometric condition.

4.2. Profiles of nitrogen containing species

4.2.1. NO_2 and NO

Figure 3 shows the evolution of NO_2 and NO profiles as a function of temperature for methane oxidation in the presence of NO_2 (left) and NO (right), respectively. In the presence of 400 ppm NO_2, the consumption of NO_2 is approximately similar for all investigated equivalence ratios. The increase of the NO mole fraction is quite sharp over the range 800–900 K, and is independent of equivalence ratio. After that, it attains a "plateau" level of 280 ppm in stoichiometric and oxidizing conditions and 300 ppm in reducing conditions, with the increase of temperature. Only under rich conditions the NO concentration drops from 300 to 100 ppm when the temperature increases from 1100 K to 1200 K. The model accurately predicts the onset for both the consumption of NO_2 and production of NO. It overestimates the amount of NO when the temperature is above 800 K.

In the presence of NO (500 ppm), the mole fraction of NO_2 peaks at 850 K, which corresponds to the maximum consumption of NO with all equivalence ratios. The amount of NO_2 drops gradually as the temperature is above 850 K, meanwhile, the mole fraction of NO increases to a stable value until the temperature is beyond 900 K. Under reducing conditions, the mole fraction of NO decreases dra-

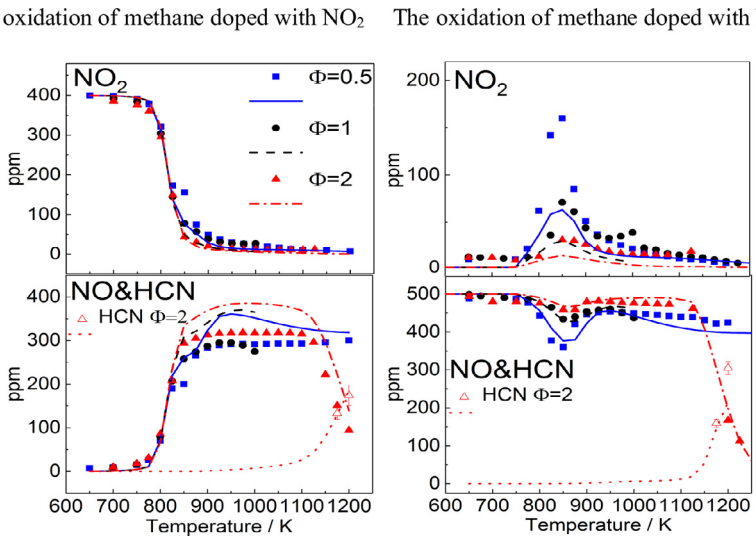

Fig. 3. The comparison of NO_2, NO and HCN profiles between experimental data and model predictions. Left: the oxidation of methane doped with NO_2 (400 ppm). Right: the oxidation of methane doped with NO (500 ppm).

matically over the temperature range 1100–1200 K. Although the model underestimates the formation of NO_2, the initiation temperature for NO–NO_2 conversion is well captured.

4.2.2. HCN

HCN has been quantified by FTIR at the highest temperatures (1175–1200 K) studied in this work for both NO_2 and NO additions as shown in Fig. 3. The measured HCN spectrum is displayed in SM1. At a same temperature, the amount of HCN is higher in the presence of NO than with NO_2 addition. Moreover, the quantification of HCN could somewhat help to close the nitrogen balance at the highest temperatures. The model predicts the formation of HCN quite well in the presence of NO_2, although it underestimates the amount of HCN in the presence of NO at 1200 K.

The mass balance of nitrogen deteriorates with the increase of temperature when temperature is above 850 K in the presence of NO_2 condition. The reason could be ascribed to the detection failure for some nitrogenated species with the currently available diagnostic instruments. Also, the overprediction of NO in the presence of NO_2 indicates that the NO_2 conversion channel needs to be further investigated.

4.2.3. A search for HONO and CH_3NO_2 species

The absorption spectrum of HONO has been previously measured by Jain et al. [33]. This previous work indicates that HONO, if any, should be detected in the present study. In our study, the cw-CRDS product analyses were conducted in the near infrared at wavenumbers in the 6638.0–6643.5 cm^{-1} range. The absorption line at 6643.17 cm^{-1} was chosen as the most suitable for the quantification of HONO with an absorption cross-section of $4.2 \pm 1.7 \times 10^{-21}$ cm^2 [33] due to the fact that there are no interferences at this specific absorption line. There were obvious signals at this absorption line in the spectrum around a temperature of 850 K. However, for some less intense absorption lines, such as 6642.45 cm^{-1}, no signals could be observed in our spectra. Therefore, the maximum produced HONO mole fraction is then below the estimated detection limit of 3 ppm. No obvious FTIR absorption lines for CH_3NO_2 could be observed. The maximum produced CH_3NO_2 mole fraction is then below the estimated detection limit of 5 ppm. The measured spectra of HONO and CH_3NO_2 of this study can be found in SM1. Modeling calculations (see SM1) predict low mole fraction (1–2 ppm) of HONO, which is consistent with what is observed in these experimental data. Note that the discrepancy between experimental and modeling calculations found in the 800–1000 K range for NO_2 (right upper in Fig. 3), can be explained by the too high predicted formation of CH_3NO_2. However, no experimental detection of this species by FTIR was achieved although it could be done.

4.3. Discussion

Reaction rate and sensitivity analyses have been performed to identify the main reaction routes and the utmost sensitive reactions for CH_4 consumption in the presence of NO_x, respectively, as shown in Fig. 4. The characteristic temperature of 850 K is selected because the consumption of methane is quite significant and the formation of carbon species peaks at this specific temperature.

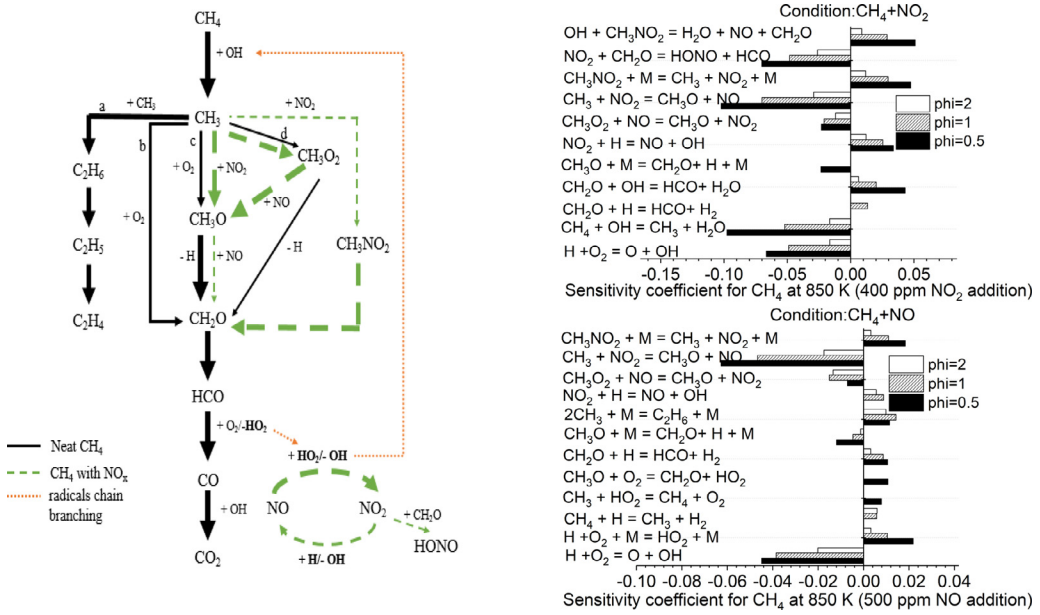

Fig. 4. Left: Reaction path diagram for CH_4 oxidation in presence of NO_x ($\Phi = 1$, $T = 850$ K). Solid lines represent the main reaction routes occurring during the oxidation of neat CH_4 (1100 K); dashed lines highlight the main changes due to the presence of NO_x. The size of the arrow is proportional to the flow rate of the given reactions. Right: CH_4 sensitivity coefficient at 850 K in the presence of NO_2 (upper: 400 ppm) and NO (bottom: 500 ppm).

In the case of neat CH_4, the reaction path analysis is conducted at 1100 K, its consumption proceeds through methyl radicals (CH_3) which can continue reacting following 4 different routes: (a) a self-reaction forming ethane; reactions with O_2, (b) forming directly $CH_2O + OH$ radicals, (c) giving CH_3O radicals which also lead to formaldehyde via reaction (1) $CH_3O(+M) = CH_2O + H(+M)$ or (d) producing CH_3O_2 radical via reaction (2) $CH_3 + O_2(+M) = CH_3O_2(+M)$, which is also a minor source of formaldehyde.

At 850 K, in the presence of NO_x, methoxy radical formation through reaction (3) $CH_3 + NO_2 = CH_3O + NO$ is the most sensitive as shown in sensitivity analysis except for the addition of NO under reducing condition, when reaction (3) is slightly less sensitive than chain branching reaction $H + O_2 = O + OH$. In this case, CH_3O radicals are also formed in large extent by the reaction of NO with CH_3O_2 radicals: reaction (4) $CH_3O_2 + NO = CH_3O + NO_2$. The whole reaction cycle (1)–(4) results in an overall balance: $2CH_3 + O_2 = 2CH_2O + 2H$ and produces a strong acceleration of methane oxidation, since 2 H atoms are obtained from 2 CH_3 radicals and one O_2 molecule. The reaction route involving C_2 species becomes more relevant as the temperature is increased being almost negligible at 850 K.

The above mentioned reaction loop (1)–(4) acts as a "catalytic" cycle and it can explain the fact that the addition of NO or NO_2 seems to have similar effects on promoting methane oxidation. Note that NO/NO_2 interchanging occurs via the reaction of NO and HO_2 radicals giving NO_2 and OH radicals and the reaction of NO_2 with H radicals reforming NO and OH radicals. The OH radicals produced during the $NO–NO_2$ interchanging cycle interact with CH_4 promoting its conversion, whereas the H and HO_2 radicals produced during the conversion of CH_4 (i.e. mainly through $CH_3O(+M) = CH_2O(+M) + H$ and $HCO + O_2 = CO + HO_2$) promote the $NO–NO_2$ conversion as described earlier. The role of the radicals in the mutual sensitization of the oxidation of CH_4 and NO_x has been highlighted in Fig. 4.

Moreover, in the presence of NO or NO_2, CH_3 radical is consumed by an alternative route, leading to the formation of nitromethane, CH_3NO_2. This acts as an inhibitor of the whole system for two different reasons: (i) it traps both CH_3 and NO_2, slowing down their successive reactions and the formation of the very reactive methoxy radical (CH_3O), and (ii) it also acts as an OH scavenger via $OH + CH_3NO_2 = H_2O + NO + CH_2O$.

The main formation route for HONO is from NO_2 by reactions $NO_2 + CH_2O = HONO + HCO$ and $NO_2 + HNO = HONO + NO$. It only represents 4% in the total NO_2 consumption at 850 K and $\Phi = 0.5$, hence the expected HONO mole fraction is small, which agrees with the

experimental data. However, these reactions play an essential role for the consumption of methane because the unstable HONO can readily convert to OH radical. In turn this favors the abstraction reaction $CH_4 + OH = CH_3 + H_2O$, which is the second most sensitive reaction for methane depletion in the conditions with NO_2 addition. Note that the sensitivity analysis in Fig. 4 shows a strong promoting effect of the reaction $NO_2 + CH_2O = HONO + HCO$.

At high temperatures, when HCN has been experimentally detected, NO reacts with HCCO and CH_3 radicals to form HCNO and H_2CN, respectively, and later HCN is obtained; thus, NO is reduced by means of well-known reburn type reactions [3].

5. Conclusions

In this work, the oxidation of neat methane and methane doped with NO_2 or NO at 107 kPa and temperatures of 650–1200 K with a fixed residence time of 1.5 s has been investigated in a jet-stirred reactor under oxidizing to reducing conditions from both experimental and modeling points of view. In general, there is a good agreement between experimental results and modeling calculations. New experimental data and new species detection, along with the confirmation of a detailed kinetic model under these new conditions, have provided insights into understanding the mutual effect of CH_4–NO_x interaction. The addition of NO_2 or NO produces comparable results on methane oxidation, anticipating the onset temperature for CH_4 consumption to lower temperatures (825 K) regardless of the equivalence ratio. Kinetic analysis showed that the parallel behavior of NO and NO_2 is connected to their interchanging via $NO_2 + H/CH_3 = NO + OH/CH_2O$ and $NO + HO_2/CH_3O_2 = NO_2 + OH/CH_3O$ reactions. This allows relating both actions to a common, oxidation-sensitizing mechanism, activated by methoxy radical formation, whilst counteracted by the parallel formation of nitromethane. The mole fraction of HCN has been quantified with FTIR, and the agreement between the experimental data and model predication is generally good. Modeling calculations predict the formation of CH_3NO_2, which was not detected experimentally although it could be, partially explaining the discrepancy between experimental and modeling results in the NO_2 profile at 800–1000 K. The contribution of HONO in the activation of the system was pointed out, too. The amount of HONO was under the detection limit, consistently with the modeling predictions.

Acknowledgments

This work has received funding from the European Union H2020 (H2020-SPIRE-04-2016) under Grant agreement no. 723706 and from the COST Action CM1404 “Chemistry of smart energy carriers and technologies”. Ms. Marrodán acknowledges Aragón Government for the predoctoral grant awarded.

Supplementary materials

Supplementary material associated with this article can be found, in the online version, at doi:10.1016/j.proci.2018.06.115.

References

[1] J.H. Bromly, F.J. Barnes, S. Muris, X. You, B.S. Haynes, *Combust. Sci. Technol.* 115 (1996) 259–296.
[2] M.U. Alzueta, P. Glarborg, K. Dam-Johansen, *Combust. Flame* 109 (1997) 25–36.
[3] P. Glarborg, M.U. Alzueta, K. Dam-Johansen, J.A. Miller, *Combust. Flame* 115 (1998) 1–27.
[4] A.B. Bendtsen, P. Glarborg, K.I.M. Dam-Johansen, *Combust. Sci. Technol.* 151 (2000) 31–71.
[5] P. Dagaut, J. Luche, M. Cathonnet, *Proc. Combust. Inst.* 28 (2000) 2459–2465.
[6] P. Dagaut, A. Nicolle, *Combust. Flame* 140 (2005) 161–171.
[7] C.L. Rasmussen, A.E. Rasmussen, P. Glarborg, *Combust. Flame* 154 (2008) 529–545.
[8] T. Mendiara, P. Glarborg, *Energy Fuels* 23 (2009) 3565–3572.
[9] Y.L. Chan, F.J. Barnes, J.H. Bromly, A.A. Konnov, D.K. Zhang, *Proc. Combust. Inst.* 33 (2011) 441–447.
[10] J. Giménez-López, V. Aranda, A. Millera, R. Bilbao, M.U. Alzueta, *Fuel Process. Technol.* 92 (2011) 582–589.
[11] Y. Chan, J. Bromly, A. Konnov, D. Zhang, *Combust. Sci. Technol.* 184 (2012) 114–132.
[12] J. Zhang, V. Burklé-Vitzthum, P.-M. Marquaire, *Combust. Sci. Technol.* 187 (2015) 1139–1156.
[13] J. Chai, C.F. Goldsmith, *Proc. Combust. Inst.* 36 (2017) 617–626.
[14] O. Herbinet, F. Battin-Leclerc, *Int. J. Chem. Kinet.* 46 (2014) 619–639.
[15] C. Bahrini, O. Herbinet, P.-A. Glaude, C. Schoemaecker, C. Fittschen, F. Battin-Leclerc, *Chem. Phys. Lett.* 534 (2012) 1–7.
[16] E. Ranzi, A. Frassoldati, R. Grana, et al., *Prog. Energy Combust. Sci.* 38 (2012) 468–501.
[17] W.K. Metcalfe, S.M. Burke, S.S. Ahmed, H.J. Curran, *Int. J. Chem. Kinet.* 45 (2013) 638–675.
[18] S.M. Burke, U. Burke, R. Mc Donagh, et al., *Combust. Flame* 162 (2015) 296–314.
[19] E. Ranzi, A. Frassoldati, A. Stagni, M. Pelucchi, A. Cuoci, T. Faravelli, *Int. J. Chem. Kinet.* 46 (2014) 512–542.
[20] R.X. Fernandes, K. Luther, J. Troe, *J. Phys. Chem. A* 110 (2006) 4442–4449.
[21] A. Burcat, B. Ruscic, *Third Millenium Ideal Gas and Condensed Phase Thermochemical Database for*

Combustion With Updates from Active Thermochemical Tables, Argonne National Laboratory Argonne, IL, 2005.
[22] T. Faravelli, A. Frassoldati, E. Ranzi, *Combust. Flame* 132 (2003) 188–207.
[23] A. Frassoldati, T. Faravelli, E. Ranzi, *Combust. Flame* 135 (2003) 97–112.
[24] J.A. Miller, C.T. Bowman, *Prog. Energy Combust. Sci.* 15 (1989) 287–338.
[25] L.B. Harding, S.J. Klippenstein, J.A. Miller, *J. Phys. Chem. A* 112 (2008) 522–532.
[26] N. Faßheber, J. Dammeier, G. Friedrichs, *Phys. Chem. Chem. Phys.* 16 (2014) 11647–11657.
[27] N. Lamoureux, H. El Merhubi, L. Pillier, S. de Persis, P. Desgroux, *Combust. Flame* 163 (2016) 557–575 .
[28] A.M. Dean, J.W. Bozzelli, in: Gas-phase Combustion Chemistry, Springer, 2000, pp. 125–341.
[29] R. Atkinson, D. Baulch, R. Cox, et al., *Atmos. Chem. Phys.* 6 (2006) 3625–4055.
[30] P. Glarborg, A.B. Bendtsen, J.A. Miller, *Int. J. Chem. Kinet.* 31 (1999) 591–602.
[31] CHEMKIN-PRO 15151, Reaction Design, San Diego, (2013).
[32] J. Bugler, A. Rodriguez, O. Herbinet, et al., *Proc. Combust. Inst.* 36 (2017) 441–448.
[33] C. Jain, P. Morajkar, C. Schoemaecker, B. Viskolcz, C. Fittschen, *J. Phys. Chem. A* 115 (2011) 10720–10728.